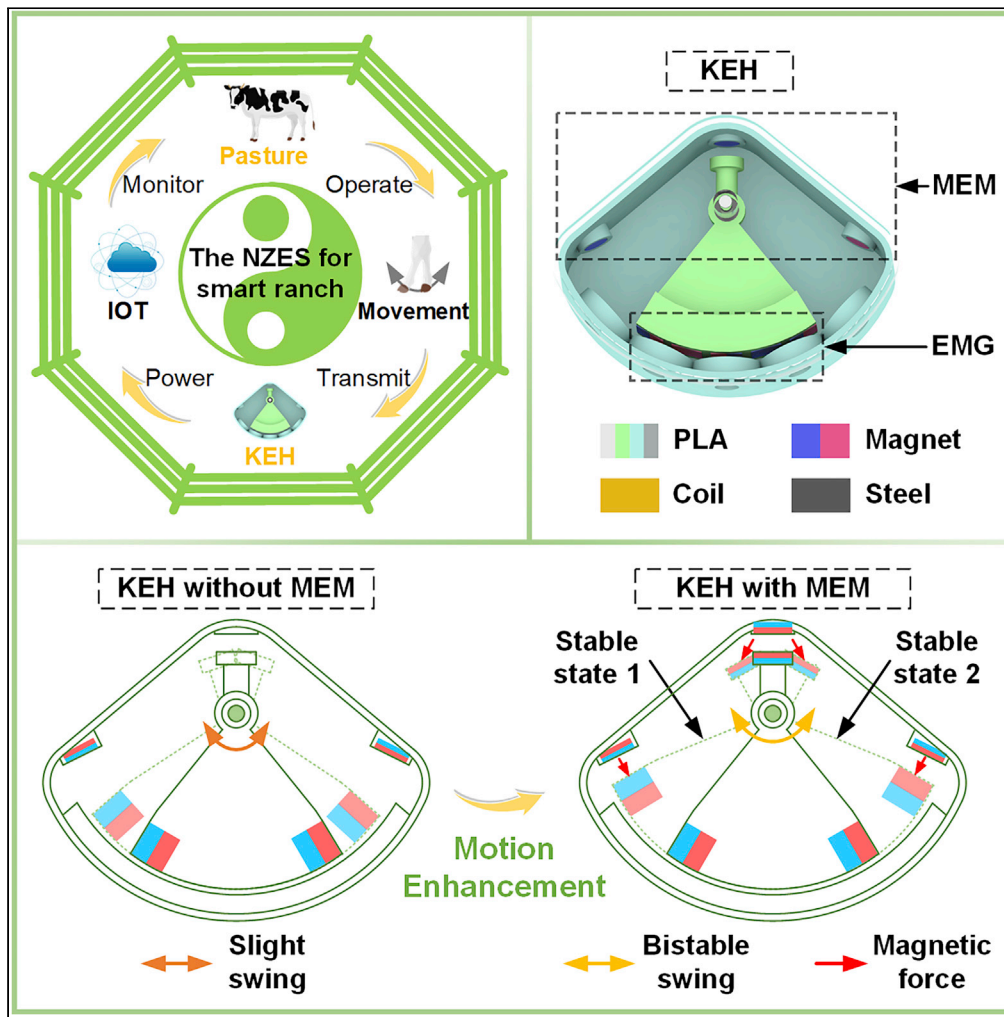


Article

A near-zero energy system based on a kinetic energy harvester for smart ranch



Lingji Kong,
Minfeng Tang,
Zutao Zhang, Yajia
Pan, Hao Cao, Xin
Wang, Ammar
Ahmed

zzt@swjtu.edu.cn (Z.Z.)
yjpan@swjtu.edu.cn (Y.P.)

Highlights

A near-zero energy system based on a KEH for smart ranch is proposed

Motion enhancement mechanism realizes bistable swing based on magnetic force

The maximum voltage growth rate is 103.7% under weak excitation

Dressing field experiments on the human body and cattle are performed

Kong et al., iScience 25,
105448
December 22, 2022 © 2022
The Author(s).
[https://doi.org/10.1016/
j.isci.2022.105448](https://doi.org/10.1016/j.isci.2022.105448)



Article

A near-zero energy system based on a kinetic energy harvester for smart ranch

Lingji Kong,^{1,2} Minfeng Tang,^{1,2} Zutao Zhang,^{1,3,*} Yajia Pan,^{1,*} Hao Cao,^{1,2} Xin Wang,^{1,2} and Ammar Ahmed²

SUMMARY

Smart ranch relying on sensor systems to realize monitoring of animals and the environment has emerged with the promotion of the Internet of Things (IoT). This paper proposes a near-zero energy system (NZES) based on a kinetic energy harvester (KEH) for smart ranch. The KEH is based on motion enhancement mechanism (MEM) for kinetic energy recovery from animal movement to realize self-powered applications of smart ranch. The MEM realizes the input and enhancement of weak kinetic energy based on bistable inertial swing. The KEH is analyzed theoretically and experimentally based on cattle leg movement. Under weak excitation (low-frequency and amplitude swing), the maximum voltage growth rate of the KEH based on the MEM reaches 103.7% compared with the linear KEH. The results of application feasibility tests, dressing field experiments, and application outlook show that the KEH has the potential to realize self-powered applications in the NZES of smart ranch.

INTRODUCTION

Smart ranch combines traditional ranch and the Internet of Things (IoT) to build a traceable system for the entire industry chain to solve food safety problems.^{1–3} The near-zero energy system (NZES) for smart ranch that harvests environmental energy for its operation is considered an ideal solution to achieve self-powered applications. The realization of smart ranch relies on many wireless wearable sensors to monitor the health status, estrus status, and location information of ranch animals.^{4,5} However, the traditional methods to power sensors mainly rely on chemical batteries, which may have the problems of difficult replacement and environmental pollution.^{6–9} The self-powered applications that harvest environmental energy for their operation are considered an ideal solution.^{10–12} Wind energy,^{13–15} solar energy,^{16–18} vibrational energy,^{19–21} and human-movements-based kinetic energy sources^{22–24} are widely used in harvesting energy for self-powered systems as alternative energy sources for batteries. In addition, various energy harvesting techniques have been developed for recovering ambient energy, such as electromagnetic energy harvester,^{25,26} piezoelectric energy harvester,^{27,28} triboelectric energy harvester,^{29,30} etc.

The ranch has abundant environmental energy, such as solar and wind, but weather conditions hinder the natural environmental energy. The movements of ranch animals, such as walking and trotting, contain significant mechanical kinetic energy, so it is a promising choice to obtain mechanical kinetic energy from these movements to power self-powered applications.

The mechanical kinetic energy of animals has received extensive attention because of its wide availability and easy integration with energy conversion mechanisms.^{31–34} Existing research on animal kinetic energy harvesting based on different energy conversion mechanisms mainly can be classified into two categories: piezoelectric and electromagnetic energy harvesters. Piezoelectric energy harvester is based on the deformation of piezoelectric materials attached to animals' bodies to generate electrical energy, and electromagnetic energy harvester achieves energy conversion through the relative movement between magnets and conductive coils.

Firstly, some piezoelectric energy harvesters for harvesting the kinetic energy of animals have been developed for animal monitoring.^{35,36} Aktakka et al.³⁷ introduced a piezoelectric energy harvester to collect energy from the wing movement of a Green June Beetle, which can achieve the power of 45 μ W. Shafer et al.³⁸ also designed a piezoelectric vibration energy harvester for wildlife in flight. Cha et al.³⁹ studied a piezoelectric energy harvester in a bimorph configuration of a bionic fishtail to power wireless communication devices. These previous efforts

¹School of Mechanical Engineering, Southwest Jiaotong University, Chengdu 610031, P. R. China

²Yibin Research Institute, Southwest Jiaotong University, Yibin 64000, P. R. China

³Lead contact

*Correspondence: zzt@swjtu.edu.cn (Z.Z.), yjpan@swjtu.edu.cn (Y.P.)
<https://doi.org/10.1016/j.isci.2022.105448>



are of great significance for advancing the research on the self-powering of animal monitoring sensors, but the input of most piezoelectric energy harvesters is linearly related to the output. Moreover, these piezoelectric energy harvesters, characterized by narrow operating bandwidth, work at non-resonant frequencies, which limits their output power. Therefore, many kinetic energy harvesters introduced nonlinear technology to improve harvesting efficiency. Qian et al.⁴⁰ introduced a bionic bistable piezoelectric energy harvester for monitoring animal state information. Compared to conventional energy harvesters, the harvester could effectively enhance the output to power animal tags. The piezoelectric energy harvesters have simple structure and high output voltage, but they have a higher internal resistance and lower power output. Moreover, the piezoelectric materials are brittle and difficult to effectively couple to the body of the animal.

Secondly, many researchers focused on self-powered animal monitoring based on electromagnetic energy harvesting.⁴¹ Gutiérrez et al.⁴² proposed a heterogeneous network to monitor the position of the herd in extreme weather environments. The electromagnetic kinetic energy harvester powered the secondary node of the network. Wu et al.⁴³ developed a multi-source energy harvester to replace batteries as well as to significantly extend the duration of wildlife tracking. The proposed innovative rotational electromagnetic generator can convert bidirectional rotary movement into unidirectional rotations for higher power output. Ren et al.⁴⁴ proposed an omnidirectional kinetic energy harvester using a novel spherical Halbach array to power wildlife monitoring systems. In the tests, the maximum power of a single coil reached 0.18 mW, which can power wildlife monitoring and positioning sensors. Zhang et al.⁴⁵ designed an eccentric vibration energy harvester for self-powered wildlife monitoring. The harvester installed on human legs and sika deer had a significant output power. Electromagnetic energy harvesters have been extensively studied due to the advantages related to their compact structure, high power output and relatively high energy density. Therefore, they can meet the power requirements of many low-power sensors.

Electromagnetic energy harvesters have great potential for harvesting animal movements to achieve self-powered applications. Several weak movements (low-frequency and amplitude swing) exist in the ranch animal's activities, especially the leg movement, and the most existing linear electromagnetic kinetic energy harvesters are inefficient in recovering the energy from these movements.⁴⁶ The frequency up-conversion (FUC) techniques^{47–50} and broadband techniques^{51–54} are effective methods for eliminating bandwidth limitations and enabling energy harvesters to achieve excellent output performance under weak excitations. Specifically, the FUC technique enables efficient conversion from low frequency to high frequency, but increases mechanical damping and energy dissipation. Broadband techniques (e.g., monostable system,⁵⁵ bistable system,⁵⁶ multi-degree-of-freedom structures,⁵⁷ and internal resonance⁵⁸) can expand the operating bandwidth of energy harvesting systems and increase the magnitude of the response, leading to increased harvesting efficiency. Therefore, broadband technology can achieve higher energy output, which is suitable for animal kinetic energy harvesting.

In summary, existing kinetic energy harvesters can extend the battery life or even achieve self-powered applications for animal monitoring. However, it should be noted that these harvesters have some challenges, which are as follows: (i) The movements of ranch animals in the feedlot are primarily weak, and the power capacity of most existing kinetic energy harvesters is low under weak excitations; (ii) There are a few pieces of research focusing on broadband technology to enhance output performance for harvesting energy from animal movements. Therefore, improving the output power by introducing broadband technology in electromagnetic energy harvesters under weak excitations will be a future hotspot in animal kinetic energy harvesting research.

Herein, combining electromagnetic generators and broadband technology, this paper proposes a kinetic energy harvester (KEH) based on a motion enhancement mechanism (MEM) for effective kinetic energy recovery from ranch animal movements. The MEM, characterized by a bistable swinging mechanism, enables an enhanced output under weak excitations, and the electromagnetic generator (EMG) based on the Halbach magnet array generates electrical energy. The KEH powers the sensors for ranch animal monitoring to achieve self-powered applications in NZES for smart ranch, as shown in [Figure 1A](#). It is foreseeable that the KEH has broad application prospects in NZES for smart ranch.

RESULTS AND DISCUSSION

System design

The proposed KEH recovers the energy of animal movements to power the wearable monitoring sensors, realizing the self-powered applications in NZES for smart ranch. As shown in [Figure 1B](#), the KEH mainly

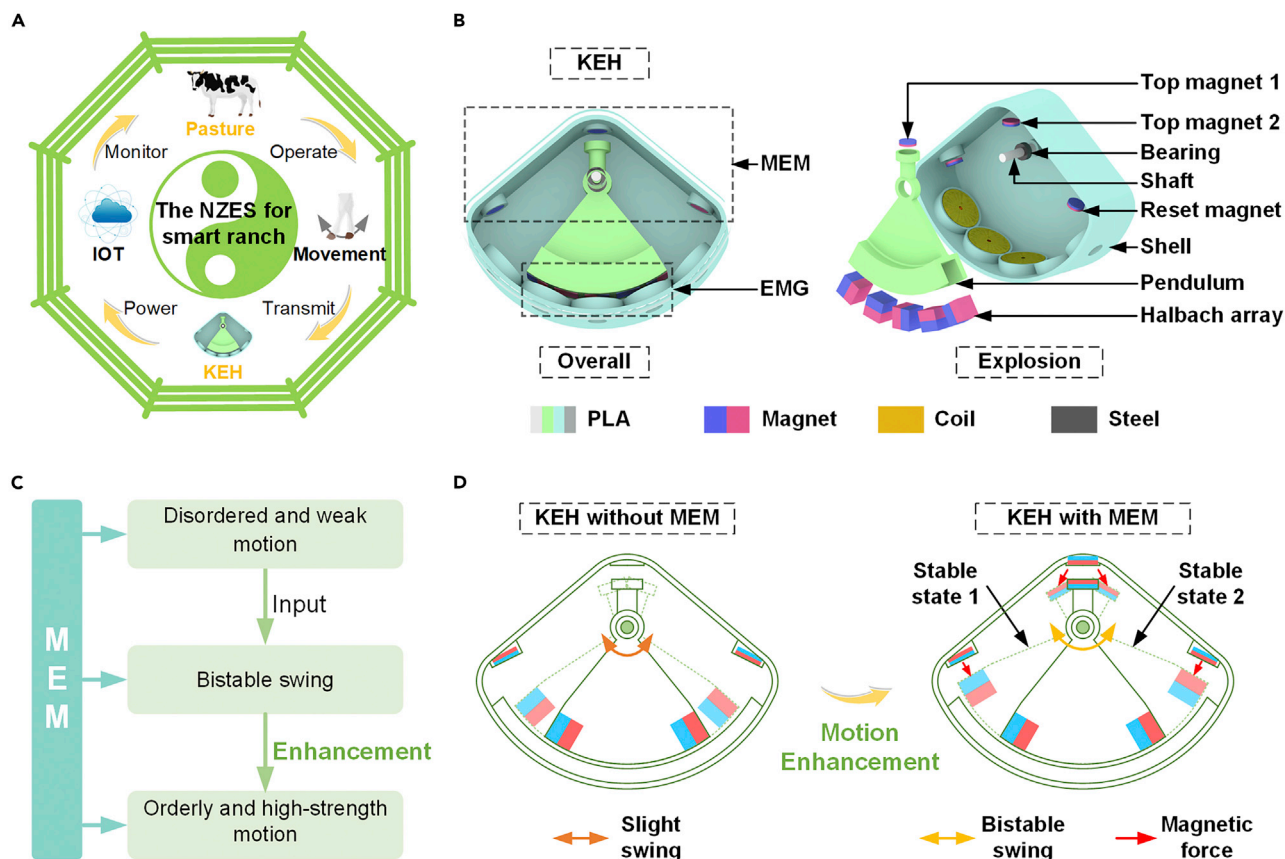


Figure 1. The proposed near-zero energy system (NZES) based on a kinetic energy harvester (KEH) for smart ranch

- (A) The KEH for self-powered applications in NZES for smart ranch.
 (B) Illustration of the KEH structure.
 (C) The outline of the motion enhancement mechanism (MEM).
 (D) Comparison of KEH with and without MEM.

consists of a MEM and an EMG. The MEM realizes the input and enhancement of kinetic energy based on bistable inertial swing, and the electromagnetic generator converts the kinetic energy into electrical energy. Furthermore, the MEM consists of a pendulum with top magnet 1, and top magnet 2 attached to the scalloped shell. The scalloped shell is fixed with the animal body, and the pendulum is matched with the shell through a bearing and a shaft. The shell moves with the movement of the animal body, and the pendulum swings around the shaft due to inertia. The rapidly reset of the pendulum is realized by two pairs of reset magnets installed on both sides of the shell and the pendulum (a pair of reset magnets is provided by the Halbach magnet array). Multi-stability, caused by the mutual repulsion of top magnet 1 and top magnet 2, enhances the pendulum's swing under weak excitations. Moreover, the EMG consists of a Halbach magnet array (installed at the lower end of the pendulum) and coils (installed at the lower end of the shell). The special magnet arrangement of the Halbach magnet array enhances the magnetic flux density for higher electrical output. As the pendulum swings relative to the shell, the coils cut the magnetic field to generate electrical energy, thereby converting the kinetic energy into electrical energy.

The movement of ranch animals contains substantial kinetic energy, and the kinetic energy harvester aims to convert disordered and weak movement into electricity. The traditional motion conversion mechanism can only realize the transformation from disordered motion to orderly motion, but cannot improve the intensity of motion. Therefore, this paper proposes a method of motion enhancement to achieve the transformation of motion and the enhancement of motion intensity, as shown in Figure 1C. The realization of the motion enhancement can rely on various methods, and the proposed MEM in this paper is based on magnet nonlinear force to realize the bistable swing of pendulum. Compared to KEH without MEM, the KEH with MEM has a larger swing speed and amplitude, as shown in Figure 1D. Therefore, the KEH with

MEM has greater potential to capture the low-intensity motion of animals. As a result, the KEH based on MEM is promising to build a smart ranch self-powered monitoring system to monitor animal health.

Modeling and analysis

In this section, the dynamics model of the KEH under a single-degree-of-freedom swing excitation is proposed, and the influencing factors of electromagnetic output performance are theoretically analyzed. Meanwhile, the potential energy of the pendulum under different conditions and the surface magnetic flux density of different magnet arrangements are compared by simulation.

The dynamics analysis of the KEH

The KEH can recover kinetic energy from animal movement. When the acceleration of the animal movement changes, the kinetic energy is converted into the pendulum's swing due to inertia. As shown in Figure 2A, the five swing states of the KEH are demonstrated. The KEH is a bistable system due to the MEM. When there is no external excitation, the KEH is in stable state 1 (state ii) or stable state 2 (state iv) due to the mutual repulsion of the top magnet 1 and the top magnet 2. When the external excitation is smaller than the potential energy barrier of the system, the pendulum can only achieve a small swing within a single trap. However, when the external excitation strength exceeds the potential energy barrier, the pendulum can achieve a swing at high speed between the two traps, meaning high energy output.

Among the movements of various parts of the animal's body, the acceleration of the leg is greater, especially in the direction of movement along the legs.³¹ Therefore, attaching the KEH to the animal's leg is a better choice as a mounting position. In this section, the kinetic behavior of the KEH based on a cattle leg movement excitation (simplified to a single-degree-of-freedom swing excitation) as a case is proposed. As shown in Figure 2B, the proposed simplified kinetic model consists of two parts: the swinging rod and the KEH. For the swinging rod, assuming that the angular acceleration of the rod is $\ddot{\alpha}$, the dynamical behavior of the KEH in a certain transient state is analyzed. With the point O_0 as the swinging center of the rod, KEH is attached to the end of the rod and moves with the rod's swing.

Therefore, the coordinates of the KEH center of gravity (point O_1) can be expressed as:

$$x_1 = L \sin \alpha \quad (\text{Equation 1})$$

$$y_1 = L \cos \alpha \quad (\text{Equation 2})$$

where L represents the distance from point O_1 to point O_0 , and α is the swing angle of the rod. Therefore, the acceleration of the point O_1 can be expressed as:

$$\ddot{x}_1 = L\ddot{\alpha}\cos \alpha - L\dot{\alpha}^2 \sin \alpha \quad (\text{Equation 3})$$

$$\ddot{y}_1 = -L\ddot{\alpha}\sin \alpha - L\dot{\alpha}^2 \cos \alpha \quad (\text{Equation 4})$$

where $\dot{\alpha}$ and $\ddot{\alpha}$ represent the angular velocity and angular acceleration of the rod, respectively.

For the KEH, the pendulum swings around the central shaft A based on a relative coordinate system under the excitation of the acceleration a ($a = -a_1$). The excitation acceleration a and the KEH acceleration a_1 have opposite direction and equal value, which can be expressed as:

$$a = -a_1 = -\sqrt{\ddot{x}_1^2 + \ddot{y}_1^2} = -\left(\ddot{x}_1 \cos \theta + \ddot{y}_1 \sin \theta\right) \quad (\text{Equation 5})$$

where θ is the instantaneous swing angle of the pendulum.

During the swinging process, the pendulum is subjected to the torque generated by the electromagnetic damping force f_e , the mechanical damping force f_r , the component of magnetic force F_m in the moving direction of top magnet 1, and gravity of the pendulum mg , so its dynamic equation can be expressed as:

$$J\ddot{\theta} = ma_l - nf_e r - f_r r_0 - mgl \sin \theta + F_m l_0 \quad (\text{Equation 6})$$

where $\ddot{\theta}$ is the angular acceleration of the pendulum, and n is the number of magnets. ma is equivalent to the inertia driving force of the pendulum, and l represents swing radius of the center of pendulum's gravity.

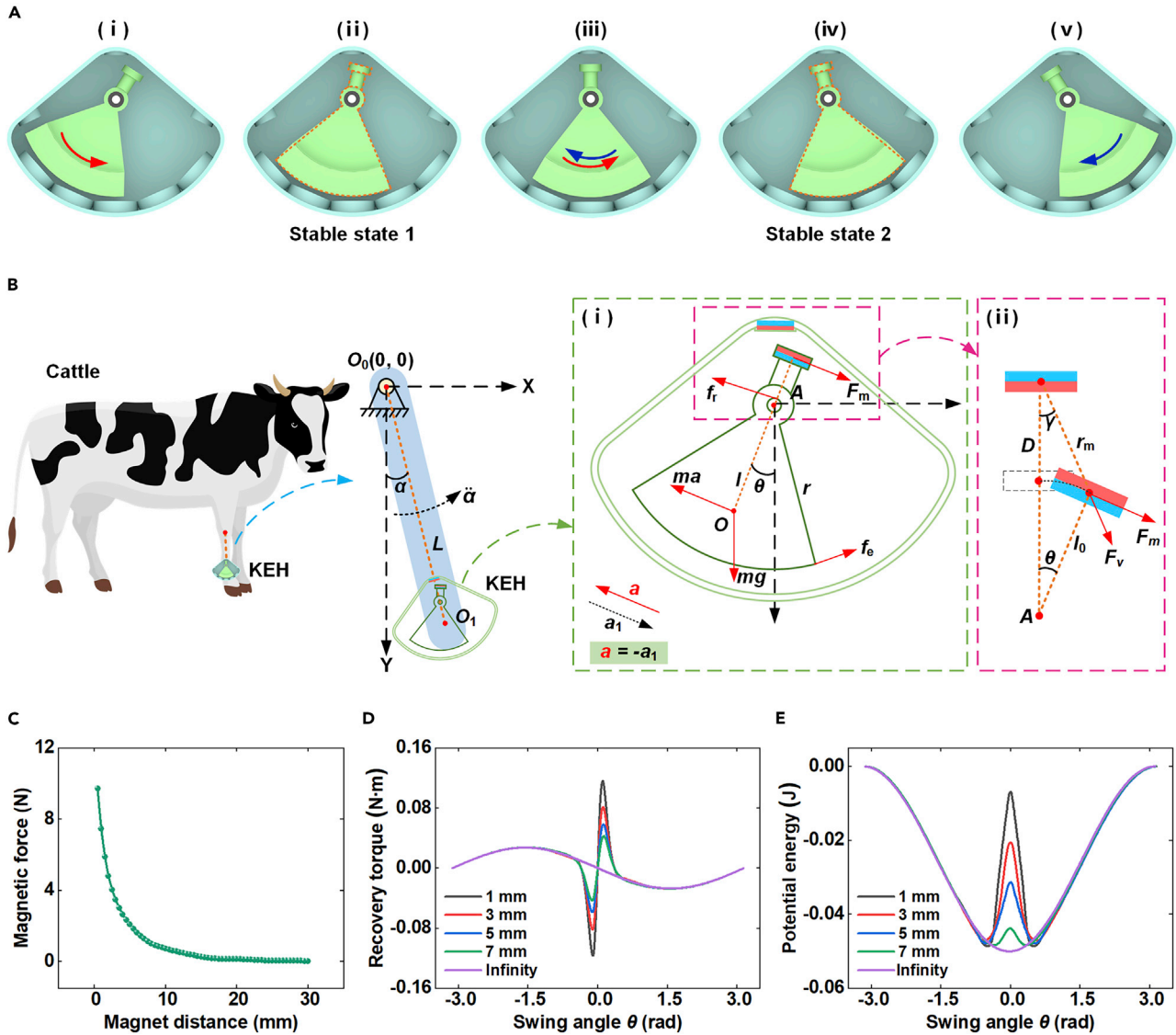


Figure 2. The theoretical analysis of the KEH

- (A) Different motion states.
- (B) A simplified kinetic model of KEH.
- (C) The change of magnet force.
- (D) The recovery torque of the pendulum.
- (E) The potential energy of the pendulum.

r , r_0 , and l_0 are the radius of the pendulum, the radius of the center shaft, and the swing radius of top magnet 1, respectively. Moreover, J is the rotational inertia of the pendulum with respect to the center of rotation, which can be given as:

$$J = I + ml^2 \quad (\text{Equation 7})$$

where I denotes the moment of inertia of the pendulum with respect to the center of gravity.

The electromagnetic damping force f_e hinders the swing of the pendulum, which can be expressed as:

$$f_e = NBI(t)l_c = NB \frac{E(t)}{R_c + R_e} l_c = \frac{NBE(t)l_c}{R_c + R_e} \quad (\text{Equation 8})$$

where N , B , and l_c are the number of turns of the coil, the magnetic field density, and the effective length of the coil cutting magnetic field, respectively. $I(t)$, $E(t)$, R_c , and R_e are the induced current, the induced voltage, the impedance of the coil, and the impedance of the external load, respectively. The mechanical damping force f_r is affected by the friction between the shaft and the bearing, which can be expressed as:

$$f_r = mgc^* \quad (\text{Equation 9})$$

where g and c^* represent the gravity acceleration and rotational damping coefficient, respectively.

F_m is caused by the mutual repulsion of the top magnet 1 and the fixed top magnet 2. By simplifying the pair of permanent magnets permanent magnets as two dipoles, F_m can be written as^{59,60}:

$$F_m = \frac{3\mu M_1 M_2}{4\pi r_m^3} [\sin \gamma + 3 \sin(\gamma + \theta) \cos \theta - 5 \sin^2(\gamma + \theta) \sin \gamma] \quad (\text{Equation 10})$$

where μ and r_m are the vacuum permeability and the distance between the centers of the two top magnets. M_1 and M_2 are the magnetic dipole moment of two magnets. From Figure 2B, r_m and γ can be expressed as:

$$r_m = \frac{D + l_0 - l_0 \cos \theta}{\cos \gamma} \quad (\text{Equation 11})$$

$$\gamma = \arcsin \frac{l_0 \sin \theta}{D + l_0 - l_0 \cos \theta} \quad (\text{Equation 12})$$

where D is the top magnet intermittent distances (vertical distance between top magnet 1 and top magnet 2).

Through the dynamics analysis above, the motion relationship of the pendulum under the single-degree-of-freedom swing excitation can be calculated.

Electromagnetic energy output analysis

The EMG consists of a Halbach magnet array and five coils, and the Halbach array consists of five same cube magnets. The Halbach array enhances the magnetic flux density through the coil, resulting in higher voltage output. To obtain the voltage response of the coils and the output power of the KEH, the magnetic flux density produced by the magnet array should be calculated. Assume a spatial point $K(x,y,z)$, whose magnetic flux density can be calculated by the following formula⁶¹:

$$B_x = \mu H_x = \frac{J^*}{4\pi} \sum_{k=0}^1 \sum_{i=0}^1 \sum_{j=0}^1 (-1)^{i+j+k} \ln(P - y + b(-1)^j) \quad (\text{Equation 13})$$

$$B_y = \mu H_y = \frac{J^*}{4\pi} \sum_{k=0}^1 \sum_{i=0}^1 \sum_{j=0}^1 (-1)^{i+j+k} \ln(P - x + b(-1)^i) \quad (\text{Equation 14})$$

where J^* is the magnetization of magnets, and b is the side length of the square magnet.

The Halbach magnet array swings around the z axis with the pendulum, and the coils are equally spaced around the z axis. Therefore, only the magnetic flux in the X axis and Y axis directions is considered. The transient magnetic flux through the coils can be given as:

$$\varphi(t) = \int \left(\sum_{i=1}^n B_x \right) ds \int \left(\sum_{i=1}^n B_y \right) ds \quad (\text{Equation 15})$$

The induced voltage of each coil can be calculated as:

$$E(t) = -N \left(\frac{d\varphi(t)}{dt} \right) \quad (\text{Equation 16})$$

Therefore, the total power $P(t)$ of the KEH can be expressed as:

$$P(t) = \frac{E^2(t)}{R_c + R_e} = \frac{N}{R_c + R_e} \left(\frac{d\varphi(t)}{dt} \right)^2 \quad (\text{Equation 17})$$

For the output power of external load, it can reach the maximum as $R_e = R_c$, and the maximal output power P_{emax} is easily obtained as:

$$P_{emax} = n \left(\frac{E(t)}{R_c + R_e} \right)^2 R_e = n \frac{E^2(t)}{4R_c} = \frac{n}{4R_c} \left(\frac{d\phi(t)}{dt} \right)^2 \quad (\text{Equation 18})$$

From the above analysis, it can be found that the parameters that affect the output power of the KEH are the rate of change of the magnetic flux of cutting the coil and the number of coils turns. Furthermore, the magnetic flux's rate of change depends on the pendulum's swing speed and the magnets' arrangement.

Potential energy analysis of pendulum

The potential energy of the pendulum is related to the recovery torque of the pendulum. In order to simplify the analysis, without considering the two parameters of mechanical damping and electromagnetic damping, the recovery torque T_r of the pendulum can be expressed as:

$$T_r = T_g - T_m = mgl \sin \theta - F_m l_0 \quad (\text{Equation 19})$$

where T_g and T_m represent the recovery torque by gravity and the recovery torque by magnetic force, respectively. According to Equation 10, the magnetic force F_m is related to the magnetic dipole moment M_1 and M_2 . Since top magnet 1 and top magnet 2 have the same configuration, the value of the magnetic dipole moment M_1 and M_2 is the same. The magnet force F_v in the direction of the line connecting the centers of the two magnets can be expressed as:

$$F_v = \frac{3\mu M_1 M_2}{4\pi r_m^3} [2 \cos \theta - 3 \sin(\gamma + \theta) \sin \gamma] \quad (\text{Equation 20})$$

As shown in Figure 2C, the magnet force F_v at different magnet distances is simulated in the COMSOL Multiphysics software, indicating that the magnet force decreases with increasing magnet distance. Therefore, the magnetic dipole moment M_1 and M_2 can be obtained by curve fitting based on Equation 20. According to the results of curve fitting, $M_1 = M_2 = 0.03 \text{ Wb} \cdot \text{m}$ is the optimal solution. According to Equation 19, the change of the recovery torque T_r with the swing angle θ under different magnet distances D (1, 3, 5, 7 mm, and infinity) are shown in Figure 2D. It can be found that there is a negative correlation between the peak value of the recovery torque and the magnet distance.

By integrating T_r from an angle $-\pi$ to π , the potential energy of the pendulum can be obtained. The potential energy curves at different magnet distances are shown in Figure 2E, which is a double-well potential energy system under the work of recovery torque by gravity and magnetic force. Different magnet distances can achieve different bistable systems, and it can be found that the potential energy barrier height decreases with the increase of the magnet distance. When the potential energy barrier height is low, the pendulum can easily overcome it under weak excitation.

Electromagnetic simulation analysis

From the previous analysis, the stronger magnetic flux density of the cutting coil can achieve a higher output power of the KEH. In this section, the COMSOL software is utilized to simulate the magnetic field of two different magnet arrangements of KEH. The magnet arrangement models, magnetic field intensity distribution cloud diagrams, and surface magnetic flux density distribution line graphs of the Halbach magnet array and the N/S pole alternate array are shown in Figures 3A–3F, respectively. The maximum and average magnetic flux density of the Halbach magnet array is stronger than the N/S pole alternate array. Therefore, the Halbach magnet array is adopted by the KEH for a larger output voltage. Based on the two-dimensional electromagnetic simulation model, the output voltage of the KEH system can be obtained by setting the swing speed of the pendulum.

Experimental result discussion

In this section, a swing test bench is designed to simulate the different movement states of a cattle's leg. The comparative experiments of the kinetic energy harvester (KEH) output performance of linear monostable and various bistable arrangements are carried out. The capacitor charging test, the optimal load experiment, the LED test, and the self-powered IoT sensor node test are carried out. To further evaluate the application performance of the KEH, human movement tests in different states and cattle movement tests in feedlot and grazing states are performed.

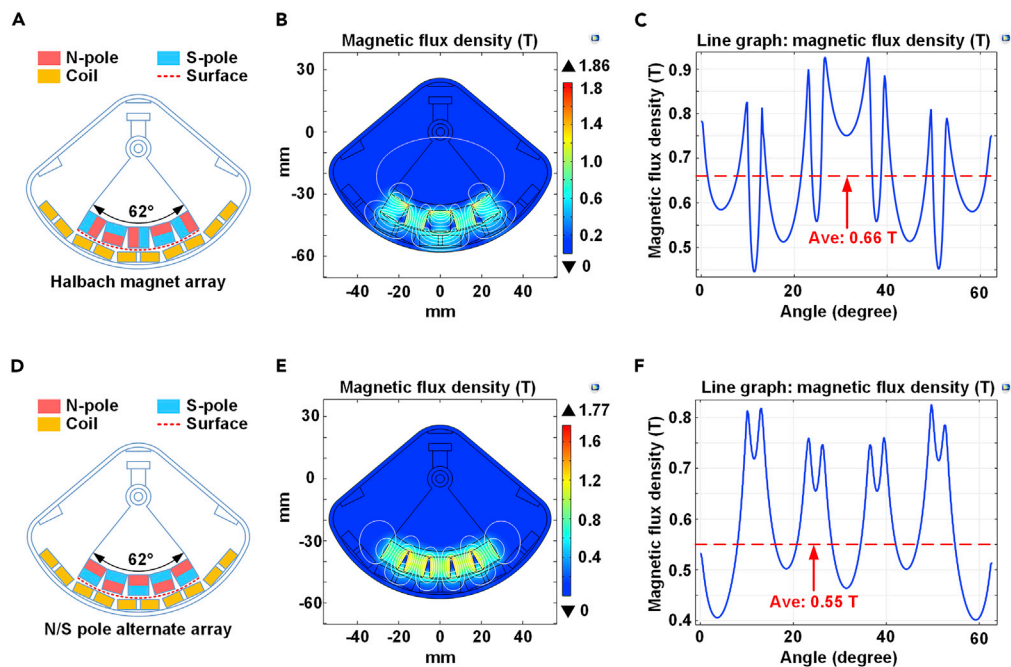


Figure 3. Comparison of magnetic field characteristics of two magnet arrangements (Halbach magnet array and N/S pole alternate array)

(A–C) (A) Magnet arrangement model, (B) magnetic field intensity distribution cloud diagrams, and (C) surface magnetic flux density distribution line graph of Halbach magnet array.

(D–F) (D) Magnet arrangement model, (E) magnetic field intensity distribution cloud diagrams, and (F) surface magnetic flux density distribution line graph of N/S pole alternate array.

Experimental setup of bench test

As shown in Figure 4, a single-degree-of-freedom swing test bench is designed to simulate the leg movement of cattle, and a 3D printing KEH prototype is manufactured. The swing test bench can be simplified as a crank-rocker mechanism with the motion principle, as shown in Figure 4A. Specifically, the crank-rocker mechanism consists of a motor-driven disk, a link, and a rocker. The direct-current motor drives the disk to rotate, and the two ends of the link are connected with the disk and the rocker, so that the rocker can swing back and forth, as shown in Figure 4B. The controller adjusts the motor speed to control the swing frequency of the rocker, and the different connect positions of the link can adjust the swing angle of the rocker (connect positions 1, 2, and 3 correspond to the swing amplitudes of 20°, 40°, and 60°, respectively). Considering the low frequency and amplitude of the leg movement, the swing excitation (frequency: 0.5–2 Hz, amplitude: 20°–60°) is adopted in the bench test. The KEH prototype is fixed to the lower end of the rocker, and the rocker swing radius is 300 mm. A resistance box (SHANE ZX99-IA) provides variable resistances, and an oscilloscope (RIGOL DS1102) is used to evaluate the output characteristics of the KEH.

The photos of the overall KEH, the shell, and the pendulum are shown in Figures 4C–4E. The KEH has dimensions of 100 mm (length) × 100 mm (width) × 30 mm (thickness) and a weight of 120 g. The shell, pendulum, and shaft are manufactured by 3D printing technology. Top magnet 1, top magnet 2, and the pair of reset magnets attached to the shell have the same dimensions of 8 mm (diameter) × 2 mm (thickness). Five cube magnets form the Halbach magnet array, which dimensions are 10 mm (length) × 10 mm (width) × 10 mm (height). Five coils (inner diameter 2 mm, outer diameter 18 mm, thickness 5 mm, and resistance 18 Ω) are equally spaced in series on the bottom of the shell. Moreover, the gap between the coil and the magnet is 3 mm.

Comparative tests of motion enhancement mechanism

The MEM is the core of KEH. The purpose of the comparison is to find the optimal steady-state arrangement (optimal top magnet distance D) of MEM under weak excitation, so that the KEH can achieve the optimal output performance. The open-circuit RMS voltage is used to evaluate the output performance

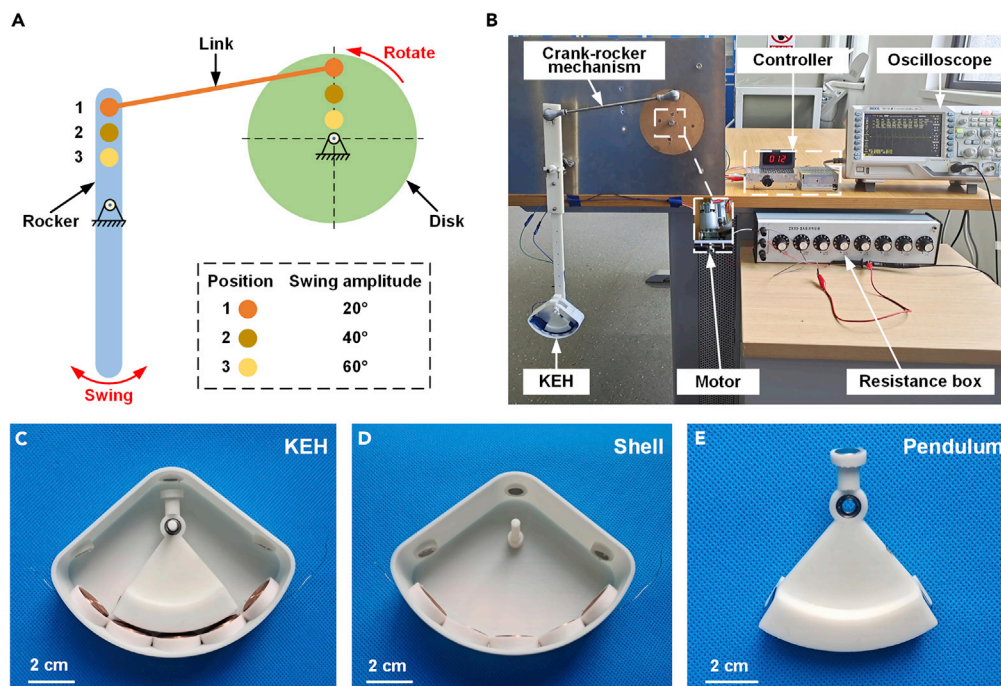


Figure 4. Experimental setup

(A) The motion principle of the crank-rocker mechanism.
 (B) The experimental scenario.
 (C–E) Photos of (C) the overall system, (D) the shell, and (E) the pendulum.

of KEH. Different top magnet intermittent distances D (vertical distance between the top magnet 1 and top magnet 2) can achieve different bistable states of the KEH. In the experiment, comparative experiments of linear monostable (distance D between top magnets 1 and 2: infinity) and various bistable arrangements (top magnet distance D : 1, 3, 5, and 7 mm) of the KEH are carried out. Figures 5A–5C compare the RMS output voltage of the KEH under different input excitations (swing frequency: 0.5–2 Hz, swing amplitude: 20°–60°).

The results intuitively show that for different excitations, the optimal magnet distance is different by comparing the RMS voltage of KEH. For example, the RMS voltage at 7 mm magnet distance is maximum at the excitation (1.5 Hz, 40°), so 7 mm is the optimal magnet arrangement for this excitation. However, under the excitation (2 Hz, 40°), 5 mm is the optimal arrangement. Combining simulation and theoretical analysis, we can draw the following conclusions from the experimental results:

- i. Under the weak excitations (0.5–1 Hz and 20°–40°), the bistable arrangements (magnet distance of 3, 5, and 7 mm) with a low potential energy barrier have a higher RMS voltage than the linear monostable arrangement of the KEH. However, the output voltage of the bistable arrangement with a magnet distance of 1 mm is low because of its high potential energy barrier. Combined with the theoretical analysis, the strength of the excitation (0.5–1 Hz and 20°–40°) is greater than the low potential energy barrier of the system ($D = 3, 5, \text{ and } 7 \text{ mm}$). Therefore, the system of bistable arrangements ($D = 3, 5, \text{ and } 7 \text{ mm}$) can overcome the potential energy barrier in the weak excitation so that it can achieve a higher voltage output. Another bistable arrangement ($D = 1 \text{ mm}$) cannot overcome the potential energy barrier because the strength of the excitation is too low, and the potential energy barrier is too high.
- ii. Under strong excitations (1.5–2 Hz and 20°–60°), the conclusion is completely different. The strength of the excitation is much greater than the potential energy barrier of the system ($D = 1, 3, 5, \text{ and } 7 \text{ mm}$). Therefore, the MEM-based bistable arrangement has almost no effect on the output performance of the EMG, so the bistable arrangement (1–7 mm) and the linear monostable arrangement (infinity) have close RMS voltage.

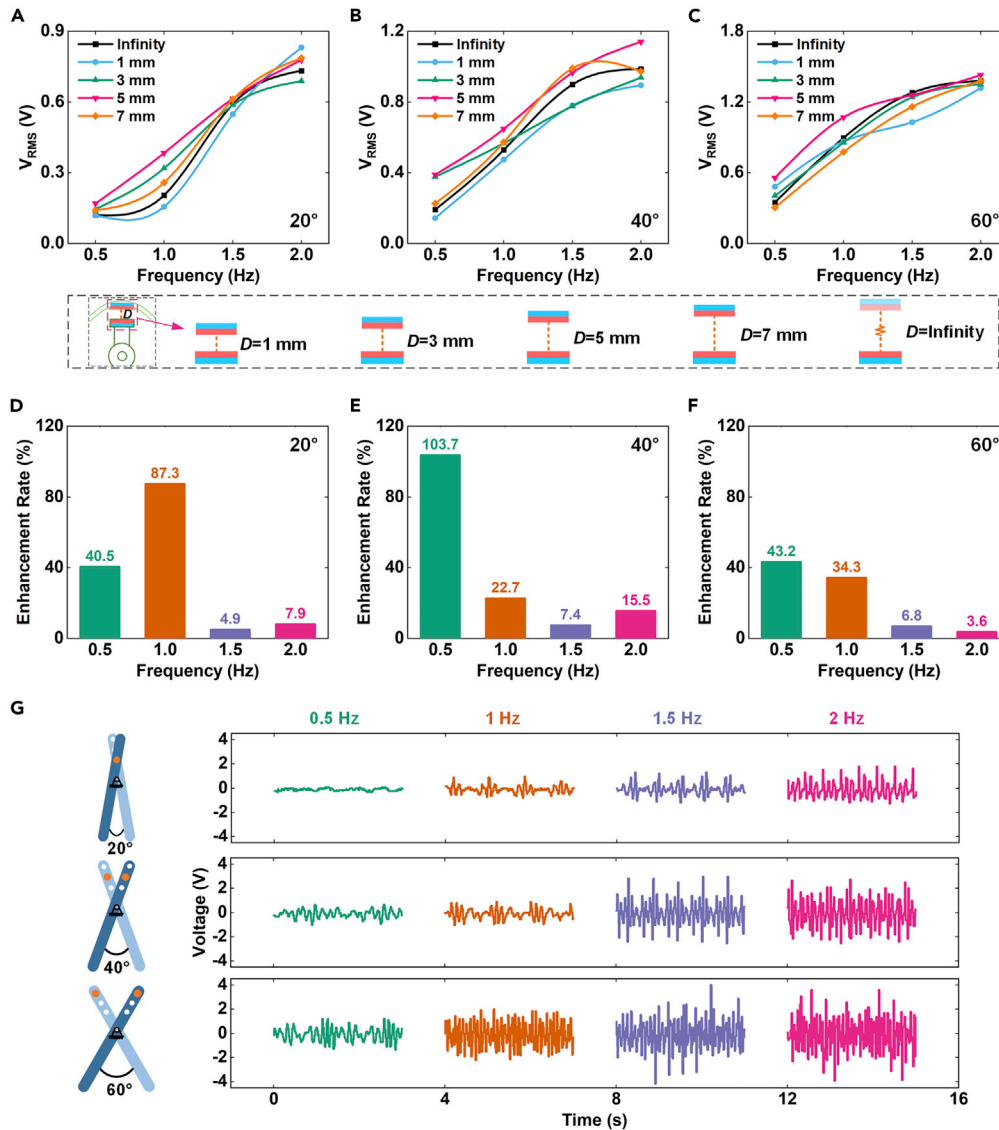


Figure 5. The KEH output performance under bench tests

(A–C) The RMS voltage output comparison under different swing excitations.

(D–F) The RMS voltage growth rate under different swing excitations.

(G) The output voltage waveform of KEH with a magnet distance of 5 mm under different excitations.

- iii. From Figures 5A–5C, at most points of the RMS voltage curve, the RMS voltage of KEH of the top magnet distance of 5 mm is the highest. Therefore, it can be deduced that 5 mm is the best bistable arrangement of the proposed KEH under the set swing excitation environment. Combined with the potential energy analysis and Figure 2E, the potential energy barrier height of the KEH system with a magnet distance of 5 mm is higher than that of the system with ($D = 7$ mm and infinity), but lower than that of the system with ($D = 1$ and 3 mm), at a moderate height. Therefore, under the excitation conditions set in the experiment, the excitation intensity is greater than the height of the potential energy barrier of the KEH system ($D = 5$ mm), so the pendulum can achieve a large swing between the double wells to achieve a better output performance.

To further analyze the movement-enhancement effects of the MEM, the voltage growth rate of the KEH ($D = 5$ mm) compared to the linear monostable arrangement of KEH is shown in Figures 5D–5F. The voltage growth rate of KEH is between 22.7% and 103.7% under weak excitation (0.5–1 Hz and 20°–60°), which is

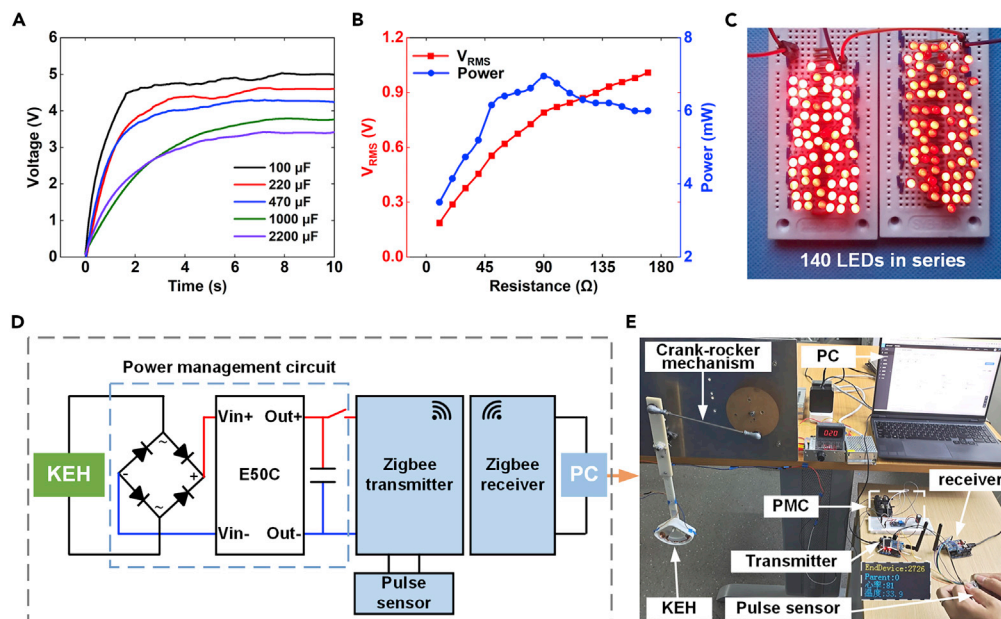


Figure 6. The output performance of the KEH under bench tests
 (A) Charging five different capacitors.
 (B) Load voltage and power of the KEH.
 (C) The KEH runs 140 LEDs in series.
 (D) The circuit diagram of the self-powered IoT sensor system.
 (E) The experimental setup of the IoT sensor system powered by KEH.

much higher than that in other environments. This shows that the electric outputs of the KEH based on the MEM are improved under weak swing excitations. Figure 5G shows the output voltage waveforms of the KEH with a magnet distance of 5 mm under different excitation conditions. It can be found that as the input excitation increases, the output voltage increases. In addition, the output voltage waveform of the KEH exhibits a chaotic state due to the nonlinear force of the top magnet. Under the swing excitation (frequency of 2 Hz, amplitude of 60°), the maximum output voltage and RMS voltage can reach 4.24 and 1.43 V, respectively, which shows the excellent output performance of KEH.

Feasibility analysis

To evaluate the actual application feasibility of the KEH, under the swing condition (2 Hz, 60°), the charging tests, the load power evaluation, the LED test, and the thermometer application test are carried out. Figure 6A shows the charging tests with several capacitors (100/220/470/1000/2200 µF), and the KEH can charge a 100 µF capacitor to 5 V in 8 s. The output voltage and power of the proposed KEH under different loads are shown in Figure 6B, and the output voltage is positively correlated with the load. Specifically, when the external load is equal to the internal resistance of the coils, the maximum output power is 7 mW. As shown in Figure 6C, 140 commercial LEDs in series are lit. The circuit diagram and the experimental setup of the self-powered IoT sensor system are shown in Figures 6D and 6E. Under swing excitation, continuous electrical energy is supplied by the KEH through a power management circuit to power a IoT sensor node. The Zigbee transmitter transmits the information monitored by the pulse sensor to the receiver, and real-time pulse information of the human body can be viewed through the computer. This proves the KEH's feasibility of harvesting kinetic energy to power IoT sensor nodes. As shown in Table 1, the proposed KEH has the advantages of motion enhancement effect and a higher output power compared with several low-frequency kinetic energy harvesters.

Performance under human and animal movements

To evaluate the performance and potential of KEH for human kinetic energy harvesting and to explore other application scenarios, the application tests of KEH are performed under human leg movement excitation.⁴⁵ As shown in Figures 7A and 7B, a triaxial accelerometer is installed at the ankle to measure the

Table 1. Comparison with several low-frequency kinetic energy harvesters

Reference	Year	Transducer	Motion conversion	Motion enhancement	Excitation condition	Average power
Zhou et al. ⁶²	2021	Electromagnetic	Eccentric pendulum	None	3.5 Hz	0.38 mW
Fan et al. ⁶³	2021	Electromagnetic	Eccentric pendulum	None	3.5 Hz	4.50 mW
Halim et al. ⁶⁴	2018	Electromagnetic	Sprung eccentric rotor	None	1 Hz	0.06 mW
Yang et al. ⁵⁰	2019	Piezoelectric	Cam and buckled-bridge	FUC technique	7.8 Hz	0.40 mW
Smilek et al. ⁶⁵	2021	Electromagnetic	Eccentric proof mass	Broadband technique	2.78 Hz	5.10 mW
This work	/	Electromagnetic	Inertia pendulum	Broadband technique	2 Hz	7.00 mW

acceleration generated by the human leg, and the KEH is mounted in the same position to recover the energy of human movement. When the human body climbs the stairs, the energy recovered by the KEH can light up the LED beads to replace reflective stickers on clothing, as shown in Figure 7C. This test demonstrates the potential of KEH for self-powered body wearable devices. The accelerations in the X axis and Y axis directions (X axis perpendicular to the tibial direction, and Y axis along the tibial direction) are measured at four different velocities of human movement, as shown in Figures 7D and 7E. From the acceleration waveform, the frequency of human leg movement is less than 2 Hz. The open-circuit output voltage waveforms of KEH at different movement speeds are shown in Figure 7F, which show that the output voltage and movement speed are positively correlated. The KEH will promote the realization of the human body's wearable self-powered monitoring.

The key technology to promote the development of smart ranch is to obtain the status information of ranch animals accurately. The KEH harvesting energy from animal movement in the ranch to power sensors is an effective way to promote the realization of NZES for smart ranch. As shown in Figures 8A–8C, the output performance of the KEH mounted on cattle's leg under different environmental conditions (feedlot and grazing) is tested. The KEH and a triaxial accelerometer are fixed to the cattle's leg by an elastic band.

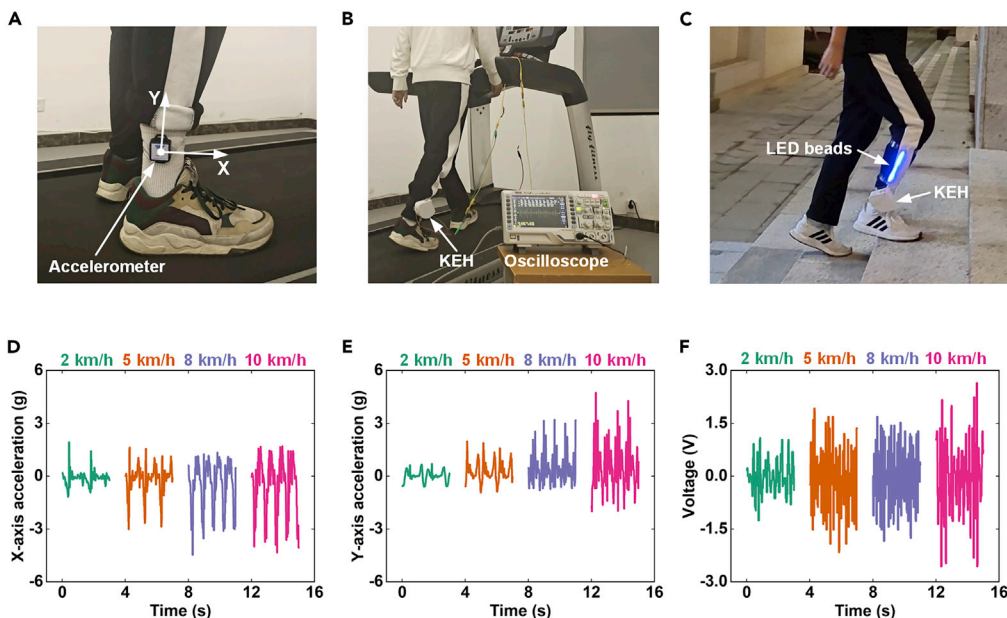


Figure 7. Application evaluation under human leg movement excitation

- (A) The mounting position of an accelerometer.
- (B) Picture of the mounting location of KEH.
- (C) KEH powers LED beads under human motion excitation.
- (D) X axis acceleration of the leg.
- (E) Y axis acceleration of the leg.
- (F) Open-circuit voltage of the KEH.

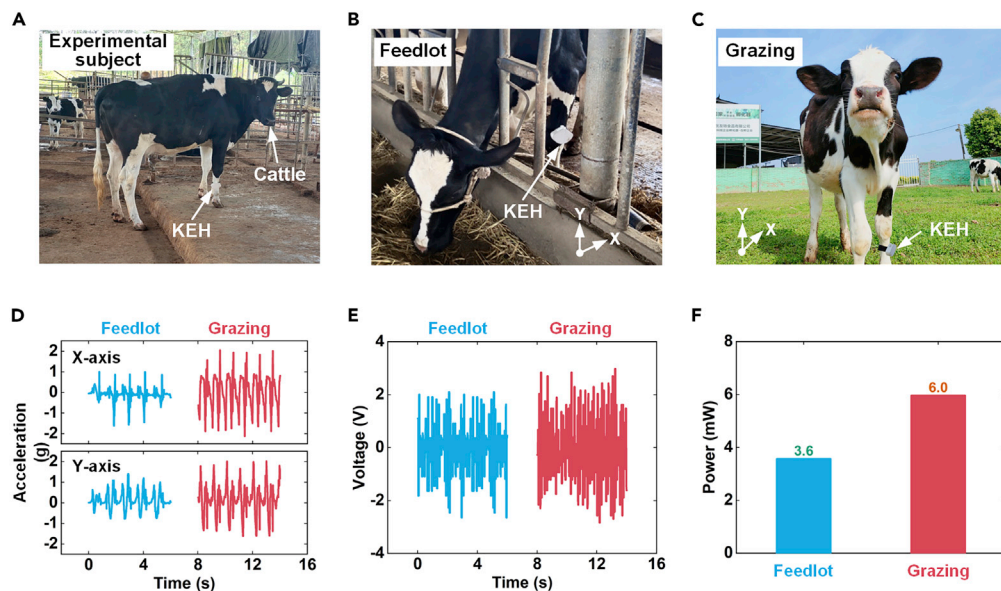


Figure 8. The performance of the KEH under cattle motion excitation

- (A) Experimental subject.
- (B) Experimental scene in feedlot.
- (C) Experimental scene in grazing.
- (D) X axis acceleration and Y axis acceleration of cattle's leg in two states.
- (E) Open-circuit voltage.
- (F) Average power in two states.

The acceleration perpendicular to the cattle leg (X axis) and along the cattle leg (Y axis) is shown in Figure 8D. It can be inferred from the acceleration waveform that the frequency of cattle is around 1 Hz, which is consistent with the experimental frequency set in the bench test section. Figure 8E is the voltage waveform of the KEH, and the result shows that the output voltage of the grazing state is high. As shown in Figure 8F, the average power in the grazing state is 6 mW, showing a good output performance. The sensor application experiments and the IoTs platform test experiments are not carried out due to the experimental conditions.

Application outlook

The power generation capacity of the KEH is related to the movement of the animals on the ranch. As shown in Table 2, based on daily cattle movement data in both grazing and feedlot environments,⁶⁶ the probable daily power generation of the KEH is 112.3 and 28.5 J under grazing and feedlot conditions, respectively. The electrical energy is used to power some potential wearable monitoring sensors in a ranch environment, as shown in Table 3. In the grazing environment, the daily power consumption of the sensors is 28.7 J, while in the feedlot environment, it is 13.5 J. It is estimated that the energy supply time of the sensors in both grazing and feedlot environments is 2.2 and 2.1 days, respectively. Possibly, the expected daily power generation of the KEH fully meets the daily power consumption of the wearable self-powered monitoring sensors.

Table 2. The expected daily power generation of the KEH

Movement state	Feedlot		Grazing	
	Time (h)	Power generation (J)	Time (h)	Power generation (J)
Standing	14.5	0	9.1	0
Lying	10.3	0	9.7	0
Walking	2.2	28.5	5.2	112.3
Total	24	28.5	24	112.3

Table 3. The probable daily power consumption of some potential self-powered monitoring sensors in the ranch

Application	Model	Power (mW)	Daily power consumption (J)	
			Feedlot	Grazing
GPS sensor	ATGM336H	26.4	0	15.2
Pulse sensor	MAX30102	9.9	3.5	3.5
Triaxial accelerometer	ADXL345	1.2	5.2	5.2
Infrared temperature sensor	GY-906	13.2	4.8	4.8
Total	–	50.7	13.5	28.7

As shown in Figure 9, the expected IoT system in the smart ranch consists of animal wearable monitoring and environmental monitoring. The designed KEH recovers animal kinetic energy and stores it in an energy storage unit through a rectifier. Based on the lasting animal kinetic energy, the energy storage unit may provide stable electrical energy for wearable monitoring sensors (including GPS, pulse transducer, triaxial accelerometer, and infrared temperature sensor). Moreover, environmental monitoring sensors may be powered by small wind turbines and photovoltaic panels. Various monitoring information in the ranch environment is sent to managers through the IoT system. The proposed KEH may have a broad prospect in the self-powered wearable monitoring of NZES for smart ranch.

According to the previous discussion, the NZES based on KEH has potential in smart ranch. In addition, since the working principle of KEH is based on inertial-triggered kinetic energy harvesting, KEH can be attached to the human body or integrated into wearable devices to recover human kinetic energy.

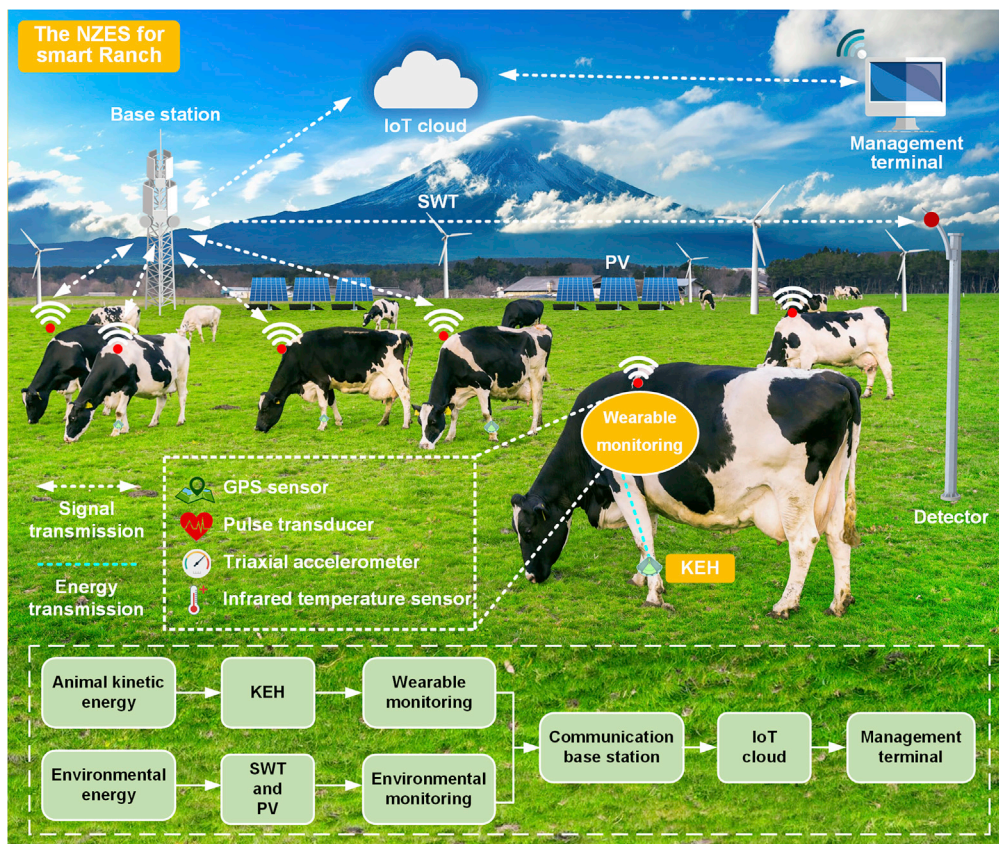


Figure 9. The expected IoT system based on the KEH in NZES for smart ranch

Therefore, the NZES based on KEH may have broad prospects in sports monitoring, healthcare, smart home, and the construction of human wireless sensor networks. In the future, it is necessary to optimize the KEH to improve the output performance and reliability, and to promote the miniaturization of the KEH for integration into smart wearable devices.

Conclusions

This work proposes a kinetic energy harvester (KEH) based on a motion enhancement mechanism (MEM) for kinetic energy recovery from animal movement, realizing self-powered applications in near-zero energy system (NZES) for smart ranch. The proposed KEH is analyzed theoretically and experimentally based on cattle leg movement as a case. The dynamic response of the KEH and the influence of different top magnet arrangements (1, 3, 5, 7 mm, and infinity) on the potential energy are analyzed. The magnetic flux distribution of different magnet arrangements is compared through simulations. A swing test bench is designed and built to simulate the leg movement of cattle, and the output response of the KEH under different swing excitations is studied. The result of the comparative tests of the MEM shows that the electric output of the proposed KEH (top magnet distance of 5 mm) is improved under weak swing excitations (frequency: 0.5–1 Hz, amplitude: 20°–60°) compared with the linear monostable arrangement of KEH, and the maximum voltage growth rate can reach 103.7%. The KEH can produce an average output power of 7 mW, sufficient to power 140 LEDs in series, charge a 100 μ F capacitor to 5 V in 8 s, and power an IoT sensor node. When the designed KEH is attached to the leg of a human or cattle, the generated electrical energy under jogging is sufficient for running a thermometer. Moreover, an application prospect of the KEH in NZES for smart ranch is performed. It demonstrates that the KEH has the potential to achieve self-powered applications and promote the sustainable development of NZES for smart ranch.

Limitations of the study

The proposed kinetic energy harvester (KEH) is analyzed theoretically and experimentally based on cattle leg movement as a case. In addition, to evaluate the performance and potential of KEH for human kinetic energy harvesting and to explore other application scenarios, the application tests of KEH are performed under human leg and cattle's leg movement excitation. However, the sensor application experiments and the IoTs platform test experiments are not carried out due to the experimental conditions in a ranch environment. In order to enhance the persuasion of smart ranch, in the future research, practical application experiments will be carried out in depth.

STAR★METHODS

Detailed methods are provided in the online version of this paper and include the following:

- KEY RESOURCES TABLE
- RESOURCE AVAILABILITY
 - Lead contact
 - Material availability
 - Data and code availability
- METHODS DETAILS
- QUANTIFICATION AND STATISTICAL ANALYSIS

SUPPLEMENTAL INFORMATION

Supplemental information can be found online at <https://doi.org/10.1016/j.isci.2022.105448>.

ACKNOWLEDGMENTS

This work was supported by the National Natural Foundation of China under Grants No. 51975490 and by the Science and Technology Projects of Sichuan under Grants Nos. 2021YFQ0055, 2021YFSY0059, 2022JDRC0075, and 2022NSFSC046; and by the Science and Technology Projects of Chengdu under Grant No. 2021YF0800138GX. Zutao Zhang and Yajia Pan are the authors to whom all correspondence should be addressed. The first two authors contributed equally to this work.

AUTHOR CONTRIBUTIONS

L.K.: Conceptualization, Methodology, Validation, Investigation, Writing-Original draft; M.T.: Software, Investigation, Writing-Original draft; Z.Z.: Supervision, Resources, Writing-Review; Y.P.: Supervision,

Resources, Writing-Review; H.C.: Data curation, Investigation; X.W.: Data curation, Investigation; A.A.: Validation, Investigation, Writing-Original draft.

DECLARATION OF INTERESTS

The author declares no competing interests.

Received: August 5, 2022

Revised: September 18, 2022

Accepted: October 24, 2022

Published: December 1, 2022

REFERENCES

- Taneja, M., Jalodia, N., Malone, P., Byabazaire, J., Davy, A., and Olariu, C. (2019). Connected cows: utilizing fog and cloud analytics toward data-driven decisions for smart dairy farming. *IEEE Internet Things Mag.* 2, 32–37. <https://doi.org/10.1109/iotm.0001.1900045>.
- Zhao, X., Askari, H., and Chen, J. (2021). Nanogenerators for smart cities in the era of 5G and Internet of Things. *Joule* 5, 1391–1431. <https://doi.org/10.1016/j.joule.2021.03.013>.
- Shi, Q., Yang, Y., Sun, Z., and Lee, C. (2022). Progress of advanced devices and internet of things systems as enabling technologies for smart homes and health care. *ACS Mater. Au* 2, 394–435. <https://doi.org/10.1021/acsmaterialsau.2c00001>.
- Zhang, J., Zhang, R., Yang, Q., Hu, T., Guo, K., and Hong, T. (2021). Research on application technology of 5G Internet of Things and big data in dairy farm. In *2021 International Wireless Communications and Mobile Computing (IWCMC)*, pp. 138–140. <https://doi.org/10.1109/IWCMC51323.2021.9498643>.
- Halachmi, I., Guarino, M., Bewley, J., and Pastell, M. (2019). Smart animal agriculture: application of real-time sensors to improve animal well-being and production. *Annu. Rev. Anim. Biosci.* 7, 403–425. <https://doi.org/10.1146/annurev-animal-020518-114851>.
- Li, J., Sharma, S., Liu, X., Pan, Y.-T., Spendlow, J.S., Chi, M., Jia, Y., Zhang, P., Cullen, D.A., Xi, Z., et al. (2019). Hard-magnet L10-CoPt nanoparticles advance fuel cell catalysis. *Joule* 3, 124–135. <https://doi.org/10.1016/j.joule.2018.09.016>.
- Tang, M., Cao, H., Kong, L., Azam, A., Luo, D., Pan, Y., and Zhang, Z. (2022). A hybrid kinetic energy harvester for applications in electric driverless buses. *Int. J. Mech. Sci.* 223, 107317. <https://doi.org/10.1016/j.jimecsci.2022.107317>.
- Li, H., Wang, X., Jiang, W., Fu, H., Liang, X., Zhang, K., Li, Z., Zhao, C., Feng, H., Nie, J., et al. (2018). Alkali metal chlorides based hydrogel as eco-friendly neutral electrolyte for bendable solid-state capacitor. *Adv. Mater. Interfaces* 5, 1701648. <https://doi.org/10.1002/admi.201701648>.
- Li, H., Wu, X., Zhang, Z., Tan, X., Pan, Y., Dai, C., Luo, D., Ahmed, A., and Xu, Y. (2022). An extended-range wave-powered autonomous underwater vehicle applied to underwater wireless sensor networks. *iScience* 25, 104738. <https://doi.org/10.1016/j.isci.2022.104738>.
- Pan, H., Qi, L., Zhang, Z., and Yan, J. (2021). Kinetic energy harvesting technologies for applications in land transportation: a comprehensive review. *Appl. Energy* 286, 116518. <https://doi.org/10.1016/j.apenergy.2021.116518>.
- Zhao, L.-C., Zou, H.-X., Wu, Z.-Y., Gao, Q.-H., Yan, G., Liu, F.-R., Wei, K.-X., and Zhang, W.-M. (2022). Dynamically synergistic regulation mechanism for rotation energy harvesting. *Mech. Syst. Signal Process.* 169, 108637. <https://doi.org/10.1016/j.ymsp.2021.108637>.
- Xu, S., Fu, X., Liu, G., Tong, T., Bu, T., Wang, Z.L., and Zhang, C. (2021). Comparison of applied torque and energy conversion efficiency between rotational triboelectric nanogenerator and electromagnetic generator. *iScience* 24, 102318. <https://doi.org/10.1016/j.isci.2021.102318>.
- Azam, A., Ahmed, A., Wang, H., Wang, Y., and Zhang, Z. (2021). Knowledge structure and research progress in wind power generation (WPG) from 2005 to 2020 using CiteSpace based scientometric analysis. *J. Clean. Prod.* 295, 126496. <https://doi.org/10.1016/j.jclepro.2021.126496>.
- Fang, Y., Tang, T., Li, Y., Hou, C., Wen, F., Yang, Z., Chen, T., Sun, L., Liu, H., and Lee, C. (2021). A high-performance triboelectric-electromagnetic hybrid wind energy harvester based on rotational tapered rollers aiming at outdoor IoT applications. *iScience* 24, 102300. <https://doi.org/10.1016/j.isci.2021.102300>.
- Wang, Y., Li, X., Yu, X., Zhu, J., Shen, P., Wang, Z.L., and Cheng, T. (2022). Driving-torque self-adjusted triboelectric nanogenerator for effective harvesting of random wind energy. *Nano Energy* 99, 107389. <https://doi.org/10.1016/j.nanoen.2022.107389>.
- Huo, Z.Y., Lee, D.M., Kim, Y.J., and Kim, S.W. (2021). Solar-induced hybrid energy harvesters for advanced oxidation water treatment. *iScience* 24, 102808. <https://doi.org/10.1016/j.isci.2021.102808>.
- Hao, D., Qi, L., Tairab, A.M., Ahmed, A., Azam, A., Luo, D., Pan, Y., Zhang, Z., and Yan, J. (2022). Solar energy harvesting technologies for PV self-powered applications: a comprehensive review. *Renew. Energy* 188, 678–697. <https://doi.org/10.1016/j.renene.2022.02.066>.
- Victoria, M., Haegel, N., Peters, I.M., Sinton, R., Jäger-Waldau, A., del Cañizo, C., Breyer, C., Stocks, M., Blakers, A., Kaizuka, I., et al. (2021). Solar photovoltaics is ready to power a sustainable future. *Joule* 5, 1041–1056. <https://doi.org/10.1016/j.joule.2021.03.005>.
- Qi, L., Pan, H., Pan, Y., Luo, D., Yan, J., and Zhang, Z. (2022). A review of vibration energy harvesting in rail transportation field. *iScience* 25, 103849. <https://doi.org/10.1016/j.isci.2022.103849>.
- Fu, H., Mei, X., Yurchenko, D., Zhou, S., Theodossiadis, S., Nakano, K., and Yeatman, E.M. (2021). Rotational energy harvesting for self-powered sensing. *Joule* 5, 1074–1118. <https://doi.org/10.1016/j.joule.2021.03.006>.
- Ahmed, A., Hassan, I., Helal, A.S., Sencadas, V., Radhi, A., Jeong, C.K., and El-Kady, M.F. (2020). Triboelectric nanogenerator versus piezoelectric generator at low frequency (<4 Hz): a quantitative comparison. *iScience* 23, 101286. <https://doi.org/10.1016/j.isci.2020.101286>.
- Guo, X., He, T., Zhang, Z., Luo, A., Wang, F., Ng, E.J., Zhu, Y., Liu, H., and Lee, C. (2021). Artificial intelligence-enabled caregiving walking stick powered by ultra-low-frequency human motion. *ACS Nano* 15, 19054–19069. <https://doi.org/10.1021/acsnano.1c04464>.
- Li, H., Chang, T., Gai, Y., Liang, K., Jiao, Y., Li, D., Jiang, X., Wang, Y., Huang, X., Wu, H., et al. (2022). Human joint enabled flexible self-sustainable sweat sensors. *Nano Energy* 92, 106786. <https://doi.org/10.1016/j.nanoen.2021.106786>.
- Hou, C., Chen, T., Li, Y., Huang, M., Shi, Q., Liu, H., Sun, L., and Lee, C. (2019). A rotational pendulum based electromagnetic/triboelectric hybrid-generator for ultra-low-frequency vibrations aiming at human motion and blue energy applications. *Nano Energy* 63, 103871. <https://doi.org/10.1016/j.nanoen.2019.103871>.

25. Liu, L., Shi, Q., Sun, Z., and Lee, C. (2021). Magnetic-interaction assisted hybridized triboelectric-electromagnetic nanogenerator for advanced human-machine interfaces. *Nano Energy* 86, 106154. <https://doi.org/10.1016/j.nanoen.2021.106154>.
26. Spreemann, D., Manoli, Y., Folkmer, B., and Mintenbeck, D. (2006). Non-resonant vibration conversion. *J. Micromech. Microeng.* 16, S169–S173. <https://doi.org/10.1088/0960-1317/16/9/s01>.
27. Azam, A., Ahmed, A., Kamran, M.S., Hai, L., Zhang, Z., and Ali, A. (2021). Knowledge structuring for enhancing mechanical energy harvesting (MEH): an in-depth review from 2000 to 2020 using CiteSpace. *Renew. Sustain. Energy Rev.* 150, 111460. <https://doi.org/10.1016/j.rser.2021.111460>.
28. Liu, L., Guo, X., Liu, W., and Lee, C. (2021). Recent progress in the energy harvesting technology-from self-powered sensors to self-sustained IoT, and new applications. *Nanomaterials* 11, 2975. <https://doi.org/10.3390/nano11112975>.
29. Li, H., Zhao, L., Meng, J., Pan, C., Zhang, Y., Zhang, Y., Liu, Z., Zou, Y., Fan, Y., Wang, Z.L., and Li, Z. (2020). Triboelectric-polarization-enhanced high sensitive ZnO UV sensor. *Nano Today* 33, 100873. <https://doi.org/10.1016/j.nantod.2020.100873>.
30. Li, H., Geng, H.-Z., Meng, Y., Wang, Y., Xu, X.-B., Ding, E.-X., Gao, J., Chen, L.-T., and Ma, S. (2014). Fabrication and test of adhesion enhanced flexible carbon nanotube transparent conducting films. *Appl. Surf. Sci.* 313, 220–226. <https://doi.org/10.1016/j.apsusc.2014.05.188>.
31. Van Herbruggen, B., Fontaine, J., Eerdeken, A., Deruyck, M., Joseph, W., and De Poorter, E. (2020). Feasibility of wireless horse monitoring using a kinetic energy harvester model. *Electronics* 9, 1730. <https://doi.org/10.3390/electronics9101730>.
32. Chamanian, S., Uluşan, H., Zorlu, Ö., Baghaee, S., Uysal-Biyikoglu, E., and Külah, H. (2016). Wearable battery-less wireless sensor network with electromagnetic energy harvesting system. *Sens. Actuators A Phys.* 249, 77–84. <https://doi.org/10.1016/j.sna.2016.07.020>.
33. Zhao, X., Wei, G., Li, X., Qin, Y., Xu, D., Tang, W., Yin, H., Wei, X., and Jia, L. (2017). Self-powered triboelectric nano vibration accelerometer based wireless sensor system for railway state health monitoring. *Nano Energy* 34, 549–555. <https://doi.org/10.1016/j.nanoen.2017.02.036>.
34. Yun, Y., Jang, S., Cho, S., Lee, S.H., Hwang, H.J., and Choi, D. (2021). Exo-shoe triboelectric nanogenerator: toward high-performance wearable biomechanical energy harvester. *Nano Energy* 80, 105525. <https://doi.org/10.1016/j.nanoen.2020.105525>.
35. Shafer, M.W., MacCurdy, R., Garcia, E., and Winkler, D. (2012). Harvestable vibrational energy from an avian source: theoretical predictions vs. measured values. *Active and Passive Smart Structures and Integrated Systems* 2012, 8341, 26–36. <https://doi.org/10.1117/12.915370>.
36. Badr, B.M., Delaney, K.R., and Dechev, N. (2015). Design of a low frequency piezoelectric energy harvester for rodent telemetry. *Ferroelectrics* 481, 98–118. <https://doi.org/10.1080/00150193.2015.1051441>.
37. Aktakka, E.E., Kim, H., and Najafi, K. (2011). Energy scavenging from insect flight. *J. Micromech. Microeng.* 21, 095016. <https://doi.org/10.1088/0960-1317/21/9/095016>.
38. Shafer, M.W., MacCurdy, R., Shipley, J.R., Winkler, D., Guglielmo, C.G., and Garcia, E. (2015). The case for energy harvesting on wildlife in flight. *Smart Mater. Struct.* 24, 025031. <https://doi.org/10.1088/0964-1726/24/2/025031>.
39. Cha, Y., Chae, W., Kim, H., Walcott, H., Peterson, S.D., and Porfiri, M. (2016). Energy harvesting from a piezoelectric biomimetic fish tail. *Renew. Energy* 86, 449–458. <https://doi.org/10.1016/j.renene.2015.07.077>.
40. Qian, F., Liu, M., Huang, J., Zhang, J., Jung, H., Deng, Z.D., Hajj, M.R., and Zuo, L. (2022). Bio-inspired bistable piezoelectric energy harvester for powering animal telemetry tags: conceptual design and preliminary experimental validation. *Renew. Energy* 187, 34–43. <https://doi.org/10.1016/j.renene.2022.01.018>.
41. Zurbuchen, A., Haeblerlin, A., Bereuter, L., Pfnigiger, A., Bosshard, S., Kernen, M., Philipp Heinisch, P., Fuhrer, J., and Vogel, R. (2018). Endocardial energy harvesting by electromagnetic induction. *IEEE Trans. Biomed. Eng.* 65, 424–430. <https://doi.org/10.1109/TBME.2017.2773568>.
42. Gutierrez, A., Dopico, N.I., Gonzalez, C., Zazo, S., Jimenez-Leube, J., and Raos, I. (2013). Cattle-powered node experience in a heterogeneous network for localization of herds. *IEEE Trans. Ind. Electron.* 60, 3176–3184. <https://doi.org/10.1109/tie.2012.2201435>.
43. Wu, Y., Zuo, L., Zhou, W., Liang, C., and McCabe, M. (2014). Multi-source energy harvester for wildlife tracking. *Active and Passive Smart Structures and Integrated Systems* 2014, 9057, 24–35. <https://doi.org/10.1117/12.2045139>.
44. Ren, L., Chen, R., Xia, H., and Ding, Z. (2017). An omni-directional kinetic energy harvester using a novel spherical Halbach array transducer. *Int. J. Appl. Electromagn. Mech.* 54, 249–262. <https://doi.org/10.3233/jae-160117>.
45. Zhang, H., Wu, X., Pan, Y., Azam, A., and Zhang, Z. (2021). A novel vibration energy harvester based on eccentric semicircular rotor for self-powered applications in wildlife monitoring. *Energy Convers. Manag.* 247, 114674. <https://doi.org/10.1016/j.enconman.2021.114674>.
46. Zou, H.-X., Zhao, L.-C., Gao, Q.-H., Zuo, L., Liu, F.-R., Tan, T., Wei, K.-X., and Zhang, W.-M. (2019). Mechanical modulations for enhancing energy harvesting: principles, methods and applications. *Appl. Energy* 255, 113871. <https://doi.org/10.1016/j.apenergy.2019.113871>.
47. Cheng, T., Li, Y., Wang, Y.-C., Gao, Q., Ma, T., and Wang, Z.L. (2019). Triboelectric nanogenerator by integrating a cam and a movable frame for ambient mechanical energy harvesting. *Nano Energy* 60, 137–143. <https://doi.org/10.1016/j.nanoen.2019.03.019>.
48. Fan, K., Wei, D., Zhang, Y., Wang, P., Tao, K., and Yang, R. (2021). A whirligig-inspired intermittent-contact triboelectric nanogenerator for efficient low-frequency vibration energy harvesting. *Nano Energy* 90, 106576. <https://doi.org/10.1016/j.nanoen.2021.106576>.
49. Zou, H.-X., Zhang, W.-M., Li, W.-B., Gao, Q.-H., Wei, K.-X., Peng, Z.-K., and Meng, G. (2017). Design, modeling and experimental investigation of a magnetically coupled flextensional rotation energy harvester. *Smart Mater. Struct.* 26, 115023. <https://doi.org/10.1088/1361-665X/aa8eb8>.
50. Yang, B., Yi, Z., Tang, G., and Liu, J. (2019). A gullwing-structured piezoelectric rotational energy harvester for low frequency energy scavenging. *Appl. Phys. Lett.* 115, 063901. <https://doi.org/10.1063/1.5110368>.
51. Rahman, M.T., Rana, S., Maharjan, P., Salauddin, M., Bhatta, T., Cho, H., Park, C., and Park, J.Y. (2021). Ultra-robust and broadband rotary hybridized nanogenerator for self-sustained smart-farming applications. *Nano Energy* 85, 105974. <https://doi.org/10.1016/j.nanoen.2021.105974>.
52. Paul, K., Amann, A., and Roy, S. (2021). Tapered nonlinear vibration energy harvester for powering Internet of Things. *Appl. Energy* 283, 116267. <https://doi.org/10.1016/j.apenergy.2020.116267>.
53. Gao, M., Wang, Y., Wang, Y., and Wang, P. (2018). Experimental investigation of non-linear multi-stable electromagnetic-induction energy harvesting mechanism by magnetic levitation oscillation. *Appl. Energy* 220, 856–875. <https://doi.org/10.1016/j.apenergy.2018.03.170>.
54. Li, M., and Jing, X. (2021). A bistable X-structured electromagnetic wave energy converter with a novel mechanical-motion-rectifier: design, analysis, and experimental tests. *Energy Convers. Manag.* 244, 114466. <https://doi.org/10.1016/j.enconman.2021.114466>.
55. Fan, K., Tan, Q., Liu, H., Zhang, Y., and Cai, M. (2019). Improved energy harvesting from low-frequency small vibrations through a monostable piezoelectric energy harvester. *Mech. Syst. Signal Process.* 117, 594–608. <https://doi.org/10.1016/j.ymssp.2018.08.001>.
56. Zou, H.-X., Li, M., Zhao, L.-C., Gao, Q.-H., Wei, K.-X., Zuo, L., Qian, F., and Zhang, W.-M. (2021). A magnetically coupled bistable piezoelectric harvester for underwater energy harvesting. *Energy* 217, 119429. <https://doi.org/10.1016/j.energy.2020.119429>.
57. Wen, H., Yang, P., Liu, G., Xu, S., Yao, H., Li, W., Qu, H., Ding, J., Li, J., and Wan, L. (2022).

- Flower-like triboelectric nanogenerator for blue energy harvesting with six degrees of freedom. *Nano Energy* 93, 106796. <https://doi.org/10.1016/j.nanoen.2021.106796>.
58. Wu, Y., Li, S., Fan, K., Ji, H., and Qiu, J. (2022). Investigation of an ultra-low frequency piezoelectric energy harvester with high frequency up-conversion factor caused by internal resonance mechanism. *Mech. Syst. Signal Process.* 162, 108038. <https://doi.org/10.1016/j.ymsp.2021.108038>.
 59. Wang, Y., Gao, M., Ouyang, H., Li, S., He, Q., and Wang, P. (2020). Modelling, simulation, and experimental verification of a pendulum-flywheel vibrational energy harvester. *Smart Mater. Struct.* 29, 115023. <https://doi.org/10.1088/1361-665X/abacaf>.
 60. Cho, J.Y., Jeong, S., Jabbar, H., Song, Y., Ahn, J.H., Kim, J.H., Jung, H.J., Yoo, H.H., and Sung, T.H. (2016). Piezoelectric energy harvesting system with magnetic pendulum movement for self-powered safety sensor of trains. *Sensor Actuator Phys.* 250, 210–218. <https://doi.org/10.1016/j.sna.2016.09.034>.
 61. Zhang, Y., Cao, J., Zhu, H., and Lei, Y. (2019). Design, modeling and experimental verification of circular Halbach electromagnetic energy harvesting from bearing motion. *Energy Convers. Manag.* 180, 811–821. <https://doi.org/10.1016/j.enconman.2018.11.037>.
 62. Zhou, N., Hou, Z., Zhang, Y., Cao, J., and Bowen, C.R. (2021). Enhanced swing electromagnetic energy harvesting from human motion. *Energy* 228, 120591. <https://doi.org/10.1016/j.energy.2021.120591>.
 63. Fan, K., Hao, J., Wang, C., Zhang, C., Wang, W., and Wang, F. (2021). An eccentric mass-based rotational energy harvester for capturing ultralow-frequency mechanical energy. *Energy Convers. Manag.* 241, 114301. <https://doi.org/10.1016/j.enconman.2021.114301>.
 64. Halim, M.A., Rantz, R., Zhang, Q., Gu, L., Yang, K., and Roundy, S. (2018). An electromagnetic rotational energy harvester using sprung eccentric rotor, driven by pseudo-walking motion. *Appl. Energy* 217, 66–74. <https://doi.org/10.1016/j.apenergy.2018.02.093>.
 65. Smilek, J., Hadas, Z., Vetiska, J., and Beeby, S. (2019). Rolling mass energy harvester for very low frequency of input vibrations. *Mech. Syst. Signal Process.* 125, 215–228. <https://doi.org/10.1016/j.ymsp.2018.05.062>.
 66. Dohme-Meier, F., Kaufmann, L.D., Görs, S., Junghans, P., Metges, C.C., Van Dorland, H.A., Bruckmaier, R.M., and Mürger, A. (2014). Comparison of energy expenditure, eating pattern and physical activity of grazing and zero-grazing dairy cows at different time points during lactation. *Livest. Sci.* 162, 86–96. <https://doi.org/10.1016/j.livsci.2014.01.006>.

STAR★METHODS

KEY RESOURCES TABLE

REAGENT or RESOURCE	SOURCE	IDENTIFIER
Software and algorithms		
Microsoft Visio 2019	Microsoft	https://www.microsoft.com/zh-cn/microsoft-365/visio/flowchart-software
MATLAB 2020a	Mathworks	https://www.mathworks.com/products/matlab.html
COMSOL Multiphysics 5.6	COMSOL	https://cn.comsol.com/
Other		
DS1102Z-E digital oscilloscope	RIGOL	https://rigol.com

RESOURCE AVAILABILITY

Lead contact

Further information and requests for resources and reagents should be directed to and will be fulfilled by the lead contact Zutao Zhang (zzt@swjtu.edu.cn).

Material availability

This study did not generate new unique reagents.

Data and code availability

- All data reported in this paper will be shared by the [lead contact](#) upon reasonable request.
- This paper does not report original code.
- Any additional information required to reanalyze the data reported in this paper is available from the [lead contact](#) upon request.

METHODS DETAILS

All methods can be found in the main text. Please check the [system design](#) for the design details of the system. Please check the [modeling and analysis](#) for the simulation and theoretical analysis details of the system. For details of the experimental design and device performance, please refer to the [experimental result discussion](#). Please check the [application outlook](#) for the application potential of the device.

Microsoft Visio 2019 is used to generate the visual images in the manuscript. MATLAB 2019a is used to process experimental data and generate visual images in the manuscript. The dynamic modeling software COMSOL Multiphysics 5.6 is utilized to simulate the magnetic field distribution. An oscilloscope (RIGOL DS1102) is used to evaluate the output characteristics of the device. Moreover, a demo video is provided to introduce the whole paper more vividly, as shown in [Video S1](#).

QUANTIFICATION AND STATISTICAL ANALYSIS

Microsoft Visio 2019 is used to generate the visual images in the manuscript. MATLAB 2019a is used to process experimental data and generate visual images in the manuscript. The dynamic modeling software COMSOL Multiphysics 5.6 is used to simulate magnetic flux distribution and magnet force. The voltage signals are captured by the digital oscilloscope (RIGOL DS1102).